Featuring work from the Microfluidic Systems and bioengineering laboratory of Fabrice Navarro, CEA LETI, Technologies for healthcare and biology division, France.

A versatile and automated microfluidic platform for a quantitative magnetic bead based protocol: application to gluten detection

A microfluidic system was developed to automatize multi-step biological assays such as ELISA for various applications. The technology uses pneumatically actuated chambers to perform all the fluidic operations for a fully automated protocol in a versatile architecture with integrated linear dilutions and optical detection for quantification.

As featured in:

See Charlotte Parent *et al.*, *Lab Chip*, 2022, **22**, 3147.

ROYAL SOCIETY OF CHEMISTRY

rsc.li/loc

Registered charity number: 207890

Lab on a Chip

PAPER

View Article Online
View Journal | View Issue

Cite this: *Lab Chip*, 2022, **22**, 3147

A versatile and automated microfluidic platform for a quantitative magnetic bead based protocol: application to gluten detection†

Charlotte Parent, *[a] Patricia Laurent,[a] Charles-Elie Goujon,[b] Xavier Mermet,[c] Armelle Keiser,[a] François Boizot,[a] Raymond Charles,[a] Lucas Audebert,[d] Yves Fouillet [a] and Myriam Cubizolles [a]

A microfluidic platform for the integration of multi-step biological assays has been developed. The presented system is a unique instrument compatible with microfluidic chips for various applications based on bead manipulation. Two examples of microfluidic cartridges are presented here. The first one contains two rows of eight chambers (40 and 80 μL), six reagent inlets, eight testing solution (calibrators and samples) inlets and eight outlets to reproduce precisely each step of a biological assay. This configuration is versatile enough to integrate many different biological assays and save a lot of development time. The second architecture is dedicated to one specific protocol and is completely automated from the standard and sample dilutions to the optical detection. Linear dilutions have been integrated to prepare automatically a range of standard concentrations and outlets have been modified for integrated colorimetric detection. The technology uses pneumatically collapsible chambers to perform all the fluidic operations for a fully automated protocol such as volume calibrations, fluid transport, mixing, and washing steps. A programmable instrument with a software interface has been developed to adapt rapidly a protocol to this cartridge. As an example, these new microfluidic cartridges have been used to successfully perform an immunoassay for gluten detection in the dynamic range of 10–30 ppm with good sensitivity (2 ppm) and specificity.

Received 8th April 2022,
Accepted 30th May 2022

DOI: 10.1039/d2lc00328g

rsc.li/loc

Introduction

Biological assays for quantitative determination of analytes are widely performed in multiple applications (clinical diagnostics, food safety, environmental applications, bioproduction, *etc.*). The most common procedure is to deliver the samples in a centralized laboratory where the time to obtain results can usually range from several hours to several days. However, many applications would need a low-cost, field-deployable device able to give quick and accurate on site results. For instance, in clinical diagnostics, the detection of cardiac biomarkers such as troponin[1] is of huge interest.[2] A portable device could improve chest pain patients' flow management in the emergency department.[3] Food safety is another broad field of application[1,4,5] where on site testing could provide fast results to isolate immediately a contaminated batch and prevent foodborne illnesses.

To answer this high demand, researchers have developed microfluidic based devices using various mechanisms for fluidic control including capillary flow,[6] digital microfluidics,[7,8] magnetic digital microfluidics,[9] optomagnetic technology,[10] centrifugal microfluidics,[11,12] and pneumatic actuation.[13,14] Among these techniques, paper based lateral flow assays (LFAs)[15] are already successful commercial systems such as glucose level measurement systems. However, this technology lacks sensitivity and cannot be applied to analytes present in very low concentrations (picomolar).

To reach low sensitivities and perform quantitative assays, conventional colorimetric enzyme linked immunosorbent assay (ELISA) remains the gold standard protocol[16] for medical applications. It relies on high affinity antibodies to precisely detect and quantify picomolar analyte molecules. Until now, however, this test is slow and complex. It is usually performed in 96 well plates and requires successive operations with large volumes of reagents, training

[a] *CEA, LETI, Technologies for Healthcare and Biology Division, Microfluidic Systems and Bioengineering Lab, Univ. Grenoble Alpes, F-38000 Grenoble, France. E-mail: charlotte.parent@cea.fr*
[b] *CEA, CEA Tech, Y.SPOT, Univ. Grenoble Alpes, F-38000 Grenoble, France*
[c] *CEA, LETI, Technologies for Healthcare and Biology Division, Univ. Grenoble Alpes, LSIV, F-38000 Grenoble, France*
[d] *CEA, LETI, Technologies for Healthcare and Biology Division, Univ. Grenoble Alpes, LS2P, F-38000 Grenoble, France*

† Electronic supplementary information (ESI) available. See DOI: https://doi.org/10.1039/d2lc00328g

personnel, prolonged incubation time and laboratory equipment (plate washer and microtiter plate spectrophotometer), hardly compatible with field applications. Pipetting robots have been developed within the last decades to automate fluidic operations and are widely used in pharmaceuticals and diagnostics. However, they are expensive, require an additional high cost microplate reader and they cannot be portable. For those reasons, they are usually not available in smaller hospitals. For in-field applications, a microfluidic system is more adapted due to its high potential integration capability. However regarding ELISA application, the complete protocol requires numerous serial and parallel operations, and thus its microfluidic integration remains challenging. As a consequence, many systems in the literature chose to integrate simplified ELISA compared to the standard ELISA-kit performed in a microplate.[17–19] For example, Chen *et al.*[20] set up a smartphone-enabled microfluidic chemiluminescence immunoassay to perform the quantification of a prostate-specific antigen (PSA) with a good LOD and dynamic range in less than 15 min, using acoustic trapping of antibody functionalized polystyrene particles. The microfluidic protocol requires no washing step but the immune complexes with beads and PSA have to be formed in microtubes prior to injection inside the microfluidic chip. More recently, a multiplexed microfluidic cartridge was developed and tested successfully.[21] This bead-based immuno-detection system allows quantification of host cell proteins (impurities) and monoclonal antibodies (target biopharmaceuticals) with an LOD = 1–10 ng mL^{-1} in less than 30 min directly from complex mixtures. A positive control is used to ensure that the test is valid. Despite this control, the test doesn't follow the classic recommendations from most ELISA kits which require a standard curve to reach quantitative results. Yet, due to the variability of the reagents, this calibration curve is crucial to assure the robustness of the results. Lots of other examples in the literature present a single channel chip allowing only one testing point.[22–24] These systems, based on a very simple microfluidic technique, are promising but they can't achieve a range of dilutions required for the standard calibration curve. Also, in many cases they don't integrate a complete ELISA with the amplification steps or washing steps for aiming a result with a high sensitivity and specificity. Some systems are proposed to integrate multiple testing points for calibration.[25,26] Nevertheless, such devices appear quite complex since they need a large number of inlets and tubing or manual pipetting operations such as nanowell based technologies.[27,28] One main challenge addressed in this work is to combine the sensitivity and the robustness of microwell plate ELISA and the simplicity of use of a point-of-care device with nearly no compromises. More precisely, in this paper we developed a generic architecture of a microfluidic system based on automatic magnetic bead manipulation to perform on-site quantification of various targets, including amplification and washing steps, the standard calibration curve and a duplication of the sample tested. Protocols based on magnetic beads[29,30] present many advantages such as a high surface-to-volume ratio,[31] the possibility to move the reaction zone inside the microfluidic chip, a simplified fabrication process, and potentially reusable chips (no antibody functionalization directly on the chip), as well as less storage problems. Furthermore, a generic microfluidic chip can be used for different targeted protocols, by adapting the bead coating. Importantly, microfluidic handling techniques need to be as efficient as the pipetting and operations performed in tubes or in microtiter plates. More precisely, bead based ELISA assays require efficient mixing, very precise dilution, bead capture, supernatant recovery, *etc.* To that aim, we rely on the use of the pneumatic actuation of a highly elastic membrane[32–34] in Ecoflex®, reported in previous work.[35] The membrane actuation enables hemispherical chambers to quickly fill or drain, for a large range of volumes (μL to mL (ref. 36)), ensuring both accurate dilution and efficient mixing. In this work, we studied the compatibility of such a configuration for magnetic bead based protocols. We show that the softness of the membrane and chamber geometry enable the precise control of the dynamic of the flow. For instance fast mixing is obtained during bead resuspension while low flow displacement is ensured during supernatant recovery. Moreover, we improved the robustness of the chip by designing hemispherical chambers on both pneumatic and fluidic layers and using plasma treatment for direct bonding during chip manufacturing. Based on the design of these double hemispherical chambers, we developed a new versatile architecture for the integration of protocols using bead manipulation. Up to six reagents can be injected in the microfluidic device and eight solutions (including calibrators and multiple samples) can be simultaneously tested. This architecture is designed to be well adapted for standard sandwich ELISA which is a major protocol for most commercials kits.

For the use of a field deployable device, we present a second architecture which integrates both linear dilution and optical detection. This architecture allows dilution from 1 to 8 to be performed for the standards and a dilution of 25 for one sample processed in duplicate.

As a proof of concept, we focus our efforts on gluten quantification. Indeed, gluten sensitivity affects around 10% of the western population.[24,37] Currently, ELISA is the method recommended by the Food and Agriculture Organization of the United Nations (FAO) and the World Health Organization (WHO). In the Codex Alimentarius,[38] the term "gluten-free" refers to foods that contain less than 20 mg kg^{-1} (or ppm for parts per million) gluten whereas the "low-gluten content" is between 20 and 100 ppm. Therefore, we choose to adapt a commercial kit (based on colorimetric detection) already certified by the regulation, and show that the precision of our chip is compatible with those regulations.

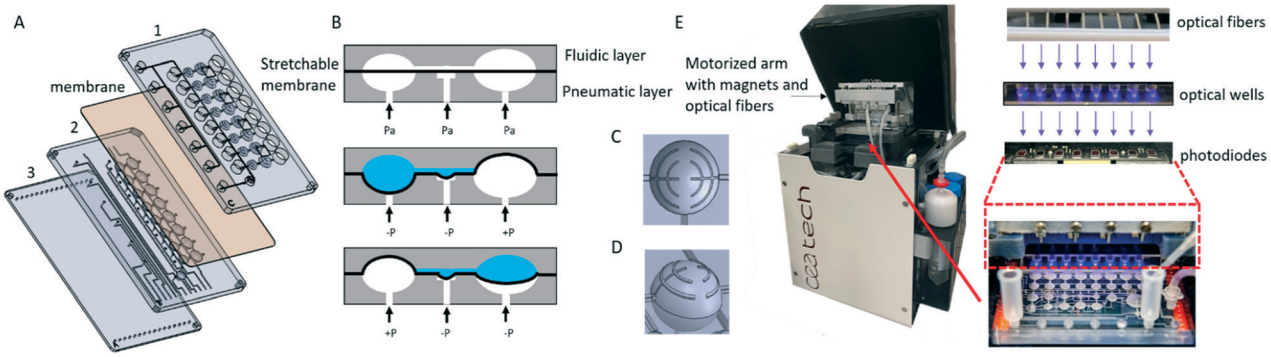

Fig. 1 Microfluidic platform design and setup: (A) exploded 3D view of the hybrid microfluidic cartridge with the fluidic layer (1), membrane, pneumatic layer (2) and cover (3), (B) cross sectional view of the microfluidic building block with a microvalve between two spherical chambers in stretchable microfluidics, (C) top view of a chamber, (D) 3D view of a chamber, and (E) microfluidic platform for pneumatic actuation and optical detection.

Materials and methods

Chip fabrication

The chip is a hybrid credit card format cartridge comprising three polymer layers and a 200 μm thick stretchable membrane (Ecoflex, Smooth, on) (Fig. 1A). This technology has been previously described for simple hemispherical chambers.[35] Microfluidic patterns are directly machined from a cyclic olefin copolymer (COC) sheet (TOPAS, US) using DATRON M7HP equipment. The stretchable membrane is positioned between the fluidic card (1) and the pneumatic card (2). In this new microfluidic cartridge, both fluidic and pneumatic layers contain hemispherical chambers to increase the volumes of interest compared to our previous study.[35] The assembly of the cartridge is done as follows. The second and the third layers are thermally bonded. To improve the precision and the robustness of the assembly, it was decided to replace the previously employed adhesive tape for the assembly with direct bonding. Therefore, the flexible membrane is plasma bonded to the pneumatic and fluidic layers following a protocol adapted from the COC to PDMS bonding.[39,40] First, the surfaces of the pneumatic and fluidic layers are activated by oxygen plasma and silanized by a 30 min immersion in a 2% 3-aminopropyltriethoxysilane (APTES) solution. Then, the layers are thoroughly rinsed with water and dried. After that, the plasma activated Ecoflex is laminated on the pneumatic level, before being covered by the fluid level. Finally, the full assembly is sealed by pressing for 15 minutes. The importance of the double hemispherical chamber design can be highlighted once again here, since it avoids direct contact of the flexible membrane with neither the pneumatic nor the fluidic layers of the chambers during the assembly process (Fig. 1B).

Fluidic actuation

The key basic building block of the microfluidic cartridge is made of at least two successive spherical collapsible chambers surrounded by microvalves (Fig. 1B). All the significant steps of the process take place in those chambers: calibrations, molecular interactions, mixing, washing, *etc.* These spherical caps are connected together with channels drilled in the fluidic layer. The pneumatic layer allows to address a positive or a negative pressure applied under the deformable membrane for each valve and chamber actuation to control flow motion throughout the chip (Fig. 1B). The fluidic layer also contains inlets (Luer holes) for the injection of the samples and reagents and various outlets (waste, recovery or detection wells).

Design rules have been implemented for successful actuation and precise fluid control. Firstly, to avoid bubble trapping and incomplete chamber draining or filling, a groove-shaped microchannel is patterned in the top chamber (Fig. 1C and D and S1†). Secondly, valve dimensions have been minimized in order to reduce dead volumes. Thus, the cylindrical bottom feature is machined to a depth of 200 μm and a diameter of 1 mm. The top feature is a spherical cap with a similar depth and diameter. With this design, a negative pressure (−150 mBar) is used to fill the chambers and valves and a positive pressure (150 mBar) to close and drain them. Furthermore to avoid leaks during fluidic transfer through the chamber networks, a higher pressure of 600 mBar is applied to the closed valves.

Microfluidic platform

A photo of this instrument is shown in Fig. 1E. The system size is 200 × 200 × 350 mm. It integrates three pressure controllers (SMC), 32 solenoid valves and homemade microcontrollers. A chip holder allows the connection between the pneumatic lines and the access ports of the microfluidic chip. For magnetic bead manipulation, a motorized arm with four magnets has been added to the instrument and is controlled vertically with an electric actuator. Down position (in contact with the chip) is used to capture magnetic beads and up position (away from the chip) for bead resuspension.

The detection system is composed of an array of eight photodiodes (SFH2240, Osram, DE) and eight optical fibers

(IDIL fibres Optiques, FR) connected to a light emitting diode (LED) at 450 nm (M455F3, Thorlabs, US) for the absorbance measurement. The optical fibers are attached to the motorized arm and aligned above the detection wells of the microfluidic chip (Fig. 1).

The platform is controlled in real time with an in house computer software (U flu factory) programmed in C++. An easy-to-use interface gives access to the different electronic components and fluidic instructions written in Python to automate the different steps.

Chip architectures

A versatile architecture (Fig. 2A) for various applications and protocols has been designed. The microfluidic platform can be programmed to perform many operations such as reagent transfer, mixing, volume calibration, washing, *etc.* This architecture consists of two rows of 8 chambers: one to calibrate the volumes (40 μL) and one where the reaction occurs (80 μL). The calibration chambers are connected to 6 reagent inlets and 8 calibrator/sample inlets. The reaction chambers are connected to 8 outlet wells for sampling prior to external detection. On the top of the reaction chambers, 4 slots allow to capture magnetic beads with permanent magnets (one slot covers two chambers). 40 valves allows to control liquid transfer. To ensure no cross contamination, the tightness of the valves has been tested. No leakage has been observed which proves the containment of each reaction. To limit the number of solenoid valves, rows of valves and chambers are actuated simultaneously thanks to the pneumatic network. 15 pneumatic channels (3 for chamber connections and 12 for valve connections) are connected through the chip manifold to solenoid valves to switch between positive and negative pressures. The versatility of this architecture allows us to choose the number of standards and samples which is an advantage for new protocol development and for sample validation but it required pipetting operations and dilution preparation before injection inside the chip.

In order to automate these operations in the point-of-care application perspective, another architecture has been designed (Fig. 2B) with the integration of the standards and sample dilutions. One sample can be tested in duplicate with this architecture. For the integration of the R-Biopharm commercial ELISA kit used to perform gluten quantification, ratios from 1/1 to 1/8 have been implemented for the calibration curve with the 1/4 ratio in duplicate for a positive control and a ratio of 1/25 for the sample preparation.

Reagent calibration and transfer

The reagent is transferred to the reaction chambers in three steps (ESI 2†). First, the pumping chamber positioned near the waste outlet (Fig. 2) allows most of the dead volumes to be filled (inlet and channels). This pumping step is done several times if necessary. Then, the calibration chambers are opened and filled precisely with reagent 1. Finally, the reaction chambers are opened while the calibration chambers are closed to allow fluid transfer (Video S6†). A second reagent can be added by repeating these steps. After incubation of a maximum of two reagents, the reaction chambers are drained through the waste outlet.

It is possible to integrate protocols based on magnetic beads in this architecture. Indeed, beads can be injected inside the reaction chambers by using this method. Antibodies immobilized on these magnetic beads enable quantitative immunoassays to be performed as described hereafter.

Dilutions

The dilution process is performed as follows: the row of chambers C3 is filled with the standard solution, while row

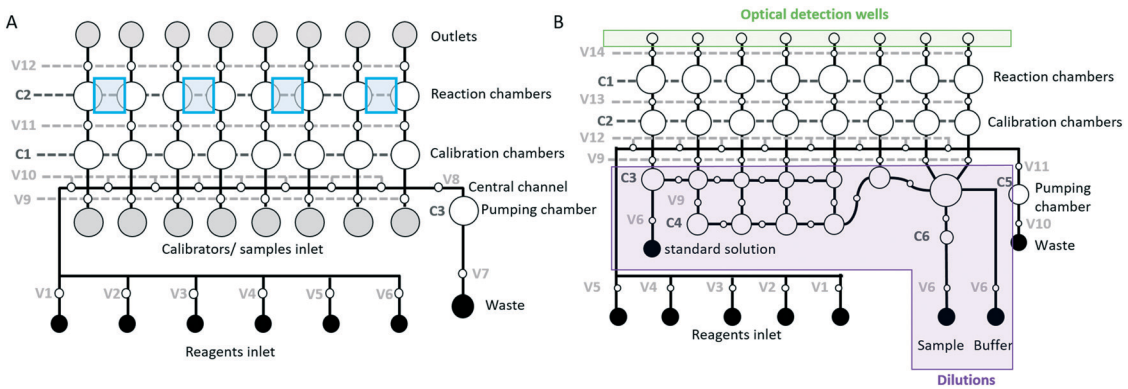

Fig. 2 Schematic views of microfluidic ELISA. (A) Versatile architecture. A row of valves (V9, V10, V11, and V12) or chambers (C1 and C2) is connected pneumatically and is actuated simultaneously. Each reagent inlet is controlled independently (from V1 to V6). C3 is a pumping chamber to prefill the central channel and drain dead volumes to waste. Eight independent inlets are used to inject calibrators and samples. The four blue slots are dedicated to the position of external magnets for magnetic bead capture. Outlets allow sample recovery for further analysis. (B) Complete ELISA architecture with integrated dilutions and optical detection. The inlet wells are replaced by two rows to prepare automatically the standard solutions and the samples by linear dilutions (purple area). The outlets are replaced by optical detection wells (green area).

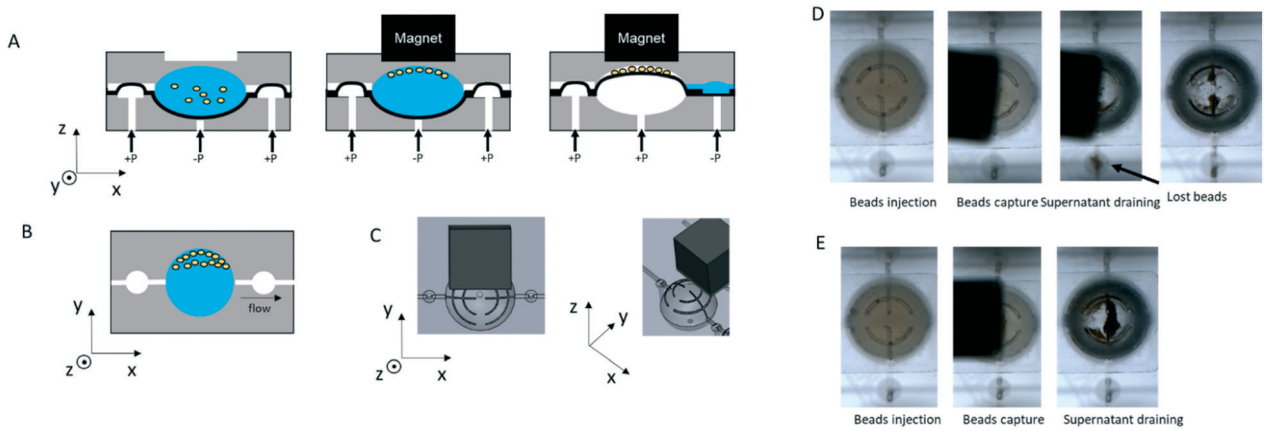

Fig. 3 Magnetic bead manipulation: (A) cross sectional schematic view during bead capture – (B) top schematic view after bead capture – (C) 3D CAD views of a reaction chamber and a magnet – comparison between two different supernatant removal: (D) without pressure steps and (E) with 15 mbar pressure steps.

C4 is filled with the buffer and chamber C6 with the sample. (ESI 3† and Fig. 2B).[35] To avoid bubble trapping, the rows are prefilled two times with the diluent and standard, respectively, and transfer to the waste before mixing.

Magnetic bead capture and washing

The key operation for a successful magnetic bead based protocol is to remove the waste supernatant without losing the beads (Fig. 3A and B). To achieve this, the magnetic force

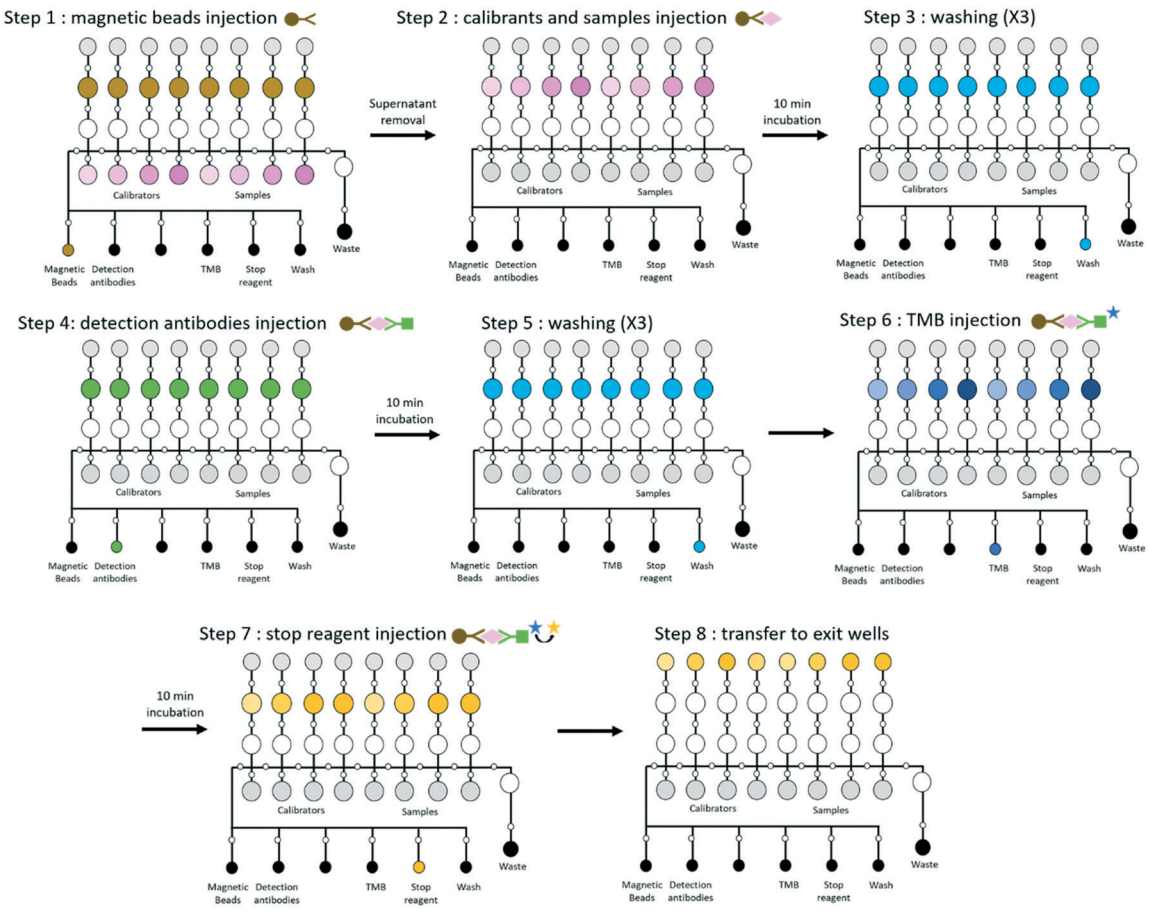

Fig. 4 Working principle to perform an ELISA assay. The figure shows a schematic top view of each step: magnetic bead injection (step 1), calibrator and sample injection (step 2), wash reagent injection (step 3), detected antibody injection (step 4), wash reagent injection (step 5), TMB injection (step 6), stop reagent injection (step 7), and transfer to the exit wells (step 8).

has to be stronger than the dragging forces on the particles during the fluid transfer. As the magnetic force is maximal near the magnet edge, the best position for the magnet is not centered but shifted to capture the beads on the chamber side (Fig. 3B and C). For this assay, we use Dynabeads® My one streptavidin (Thermo Scientific, US), and a NdFeB magnet (W-05-N, supermagnete, DE).

ELISA assay: principle and integration on the versatile architecture

RIDASCREEN® Fast gliadin ELISA test for gluten detection (R Biopharm kit, REF R7002) has been performed by using the versatile architecture. Magnetic beads (Dynabeads® My one, Thermo Scientific, US) were functionalized with capture anti-gliadin antibodies. The calibrators used in the microfluidic ELISA assay are gliadin solutions from the kit at concentrations of 0, 10, 20 and 40 ng mL^{-1}. The microwell plate provided in the kit has been used as a reference method for comparison.

This assay uses a typical ELISA procedure. The detected anti-gliadin antibodies are labelled with horseradish peroxidase (HRP) and 3,3,5,5′-tetramethylbenzidine (TMB) is the reaction substrate. The oxidation produced a yellow diimine product that absorbs light at 450 nm and it is detected by absorption spectroscopy. The absorbance values of the standards are fitted against the gliadin concentrations using a two-order polynomial regression to obtain a standard curve. Based on this calibration curve, the absorbance value of the unknown sample (or the positive control) is used to determine the gliadin concentration. Since gliadin represents 50% of the proteins present in gluten, this concentration is multiplied by 2 and by the dilution factors in order to obtain the gluten concentration in ppm.

The protocol has been adapted to be integrated in a microfluidic chip as illustrated in Fig. 4. The reagents, samples and calibrators are dispensed by hand in the reservoirs and the inlet wells. Four samples can be tested in a same experiment with this architecture. Then, the next steps are completely automated by the microfluidic platform. Reagent volumes are consecutively calibrated and transferred to the reaction chambers by using the procedure described in S1.† The motorized arm is lowered during supernatant removal operations to trap magnetic beads.

The following steps automatically come one after another: step 1 – magnetic beads are injected into the reaction chambers; step 2 – after the supernatant removal step, calibrator and sample solutions are transferred to the reaction chambers; gliadin extracted from a sample or calibration solution bonds to the captured antibodies immobilized on the magnetic beads; step 3 – after 10 min of incubation, the supernatant is removed and the beads are washed three times to eliminate unbound gliadin. Step 4 – the second antibody labelled with HRP (namely the conjugate) is added and incubated to react with the protein; step 5 – after 10 min of incubation, another 3 washing step cycles are performed; step 6 – TMB is added to initiate the colorimetric reaction; step 7 – after 10 min, the reaction is stopped with sulfuric acid; step 8 – the solutions are transferred to the exit wells. During this step, the motorized arm is down to trap the magnetic beads. Finally, 60 μL of each solution are pipetted and transferred in a microplate for absorbance measurement at 450 nm on a spectrophotometer (TECAN infinite M1000, CH). To compare the results, 60 μL issued from the kit plate was also measured in parallel in the same microplate.

At the end of the ELISA assay, a washing protocol is performed in order to reuse the microfluidic cartridge. Washing buffer is injected to the reaction chambers. A back and forth process is repeated three times to wash the stretchable chambers, the outlets and the inlets.

Integrated optical detection

In the second architecture, detection wells have been added to integrate optical detection and provide immediate results. After the stop reagent mixing step, the LEDs are turned on to a current of 800 mA and the motorized arm is lowered to capture the beads. Then the solutions are transferred to the optical wells.

The optical measurement is the ratio between the measurement of empty wells and filled wells. So before injecting the solutions, a blank measurement is performed and stored in the Python program. To generate automatically the results, the program plots a linear regression and calculates the coefficients which are used to determine the positive control and the sample concentrations.

Preparation of food samples

Gluten was extracted from various gluten-free food matrices (seeds, flours, pastes) spiked with a known concentration of wheat flour. The gluten extraction procedure was adapted from standard laboratory protocols. Briefly, gluten extraction is performed in a tube using 10 g of food matrix incubated with the extraction ethanol-based buffer.[41] Filtration of the extract (Whatman GD/X syringe filter) is performed prior to sample dilution at 1 : 25 in the ELISA buffer from the kit.

In the versatile architecture, the sample is diluted in the tube prior to its injection into the microfluidic cartridge, whereas in the complete ELISA chip the sample obtained after filtration is directly injected and subsequently diluted in the chip.

Results and discussion

Magnetic bead capture and washing

One advantage of the hyper elastic membrane combined with the pressure control is the very precise regulation of the dynamic flow which allows the collapsible chambers to be filled and drained at different velocities.

We compared two different methods for draining the supernatant. Initially, negative pressure is applied to the

chamber that is filled with a magnetic bead solution (Fig. 3D and E). To remove the supernatant, the pressure has to be switched from negative (−150 mbar) to positive (150 mBar). This operation is achieved by using the solenoid valves. However, if the pressure is switched in one-step, the liquid flow rate is too high and leads to drain magnetic beads with the supernatant (Fig. 3D). We choose to switch the pressure by an increase of 15 mbar every second. This gentle method leads to a lower flow rate and allows the magnet to capture efficiently the beads inside the chambers while removing completely the supernatant (Fig. 3E).

To validate the magnetic bead manipulation (no loss of beads, no non-specific adhesion), a simple protocol using streptavidin beads and biotin conjugated with HRP has been developed and performed (ESI 4†). By using a phosphate buffer or the commercial buffer provided in the R-Biopharm kit, magnetic beads don't show any agglomeration nor non-specific bonding on COC or Ecoflex. The transfer from the inlet to the reaction chamber thus seems efficient and the solutions appear homogeneous. The supernatant can be completely removed without losing the magnetic beads captured on the reaction chamber side. The solution is moved back and forth 5 times for bead resuspension and mixing with the reagent at each step.

To validate these observations, HRP–biotin solutions at various concentrations have been quantified by using the microfluidic chip and a microplate as a reference. The results obtained in both experiments show similar absorbance values, and the linear regression coefficients are equivalent: this validates the microfluidic protocol using magnetic beads.

ELISA: fluidic observations

A fluidic architecture with both calibration chambers and reaction chambers was set up in order to facilitate mixing by using back and forth transfers of the solutions. We observe the fluid transfer between the calibration chambers (40 μL) and the reaction chambers (80 μL). Due to the collapsible characteristic, the second chamber can be half-filled during most of the steps and completely filled after the reagent stop addition.

Small air bubbles due to dead volumes between the central channel and the chambers are present inside the calibration chambers (Fig. 5A and B). However, since they are similar for each chamber and their volumes are small compared to that of the chamber, we can assume that bubbles have no impact on the precision. However, to achieve a precise volume calibration, three cycles with the pumping chamber appear to be necessary. For a precise quantification, the samples and calibrators have to be transferred simultaneously to the reaction chambers.

ELISA: quantitative validations on the versatile architecture

The versatile architecture has been described previously in Fig. 2A. The protocol follows the fluidic steps explained in

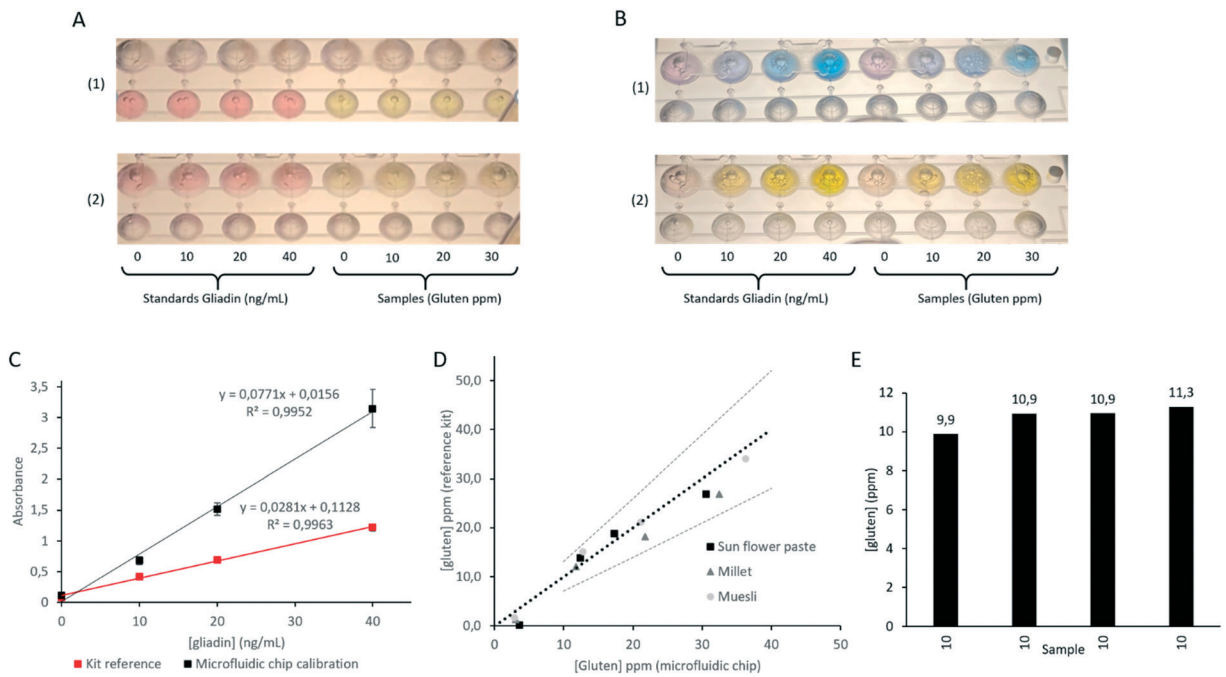

Fig. 5 Validation of an ELISA assay on the versatile architecture: (A) standards and samples transfer to the calibration chambers (1) and to the reaction chambers (2). (B) Images of the reaction chambers after mixing with TMB and 10 min of incubation (1) and after mixing with the stop reagent (2). (C) Calibration curves obtained with the reference kit and the microfluidic chip from the average of three experiments for each point (0, 10, 20 and 40 ng mL^{-1} gliadin). (D) Comparison between the reference kit and the microfluidic chip for the quantification of spiked samples. 30% error has been represented by grey dotted lines started at 10 ppm, corresponding to the limit of quantification provided in the commercial kit. (E) Quantification of 4 same samples of millet flour spiked at 10 ppm gluten.

Fig. 4. Four inlets are dedicated to gliadin standards (0, 10, 20 and 40 ng mL^{-1} gliadin) and the four additional ones are devoted to the samples to be tested at 0, 10, 20 and 30 ppm gluten (gluten extracted from millet flour, seed mix or sunflower paste). Fig. 5 and Video S7† show the solutions contained in each reaction chamber and obtained at the end of the ELISA test. The result can be seen with the naked eye but required an absorbance measurement for quantitative measurements.

For each experiment, a calibration curve is essential to quantify the results. The absorbance measurements of the standard gliadin solutions lead to this calibration curve (Fig. 5C). To assess the repeatability of such an ELISA assay, the whole microfluidic protocol has been performed three times (once for each sample mixture) on the same recycled microfluidic chip. These curves show a high linearity (R^2 = 0.9952 for the microfluidic chip test and 0.9963 for the kit reference). The absorbance intensity increased from 0.67 to 3.14 as the gliadin concentration increased from 10 to 40 ng mL^{-1}. It can be noticed that with a similar optical path, the absorbance levels are in average 2.7 higher for the microfluidic chip protocol compared to the one done using the kit.

The linear equations and the absorbance measurements of the samples can be used to quantify gliadin concentration (ng mL^{-1}) in the spiked samples and therefore calculate the gluten concentration (ppm). The experimentally calculated gluten concentration can be compared to the gluten concentration obtained with the kit (Fig. 5D and S5†). The results show that the microfluidic chip succeeded to quantify the samples since similar values to the ones of the commercial kit were obtained.

To evaluate the repeatability of our microfluidic system, four identical samples of millet flour containing 10 ppm gluten have been tested on the same chip (Fig. 5E). The results are repeatable with a standard deviation of 5.6% and this confirms the robustness of the system despite the trapping of air bubbles. These results are satisfactory since the reference kit supplier recommends that the coefficient of variation should not exceed 10%. The average error between the expected value and the experimental value is 8%. As a comparison, this error value for the results obtained with a standard kit is 3%. Based on the regulation recommendations, both the chip and kit results are good since they are in the expected recovery range (70–130%) of the check sample.

Fully integrated and automated ELISA with on chip optical detection

To validate the architecture with integrated dilution and optical detection, a sample of millet flour spiked with 10

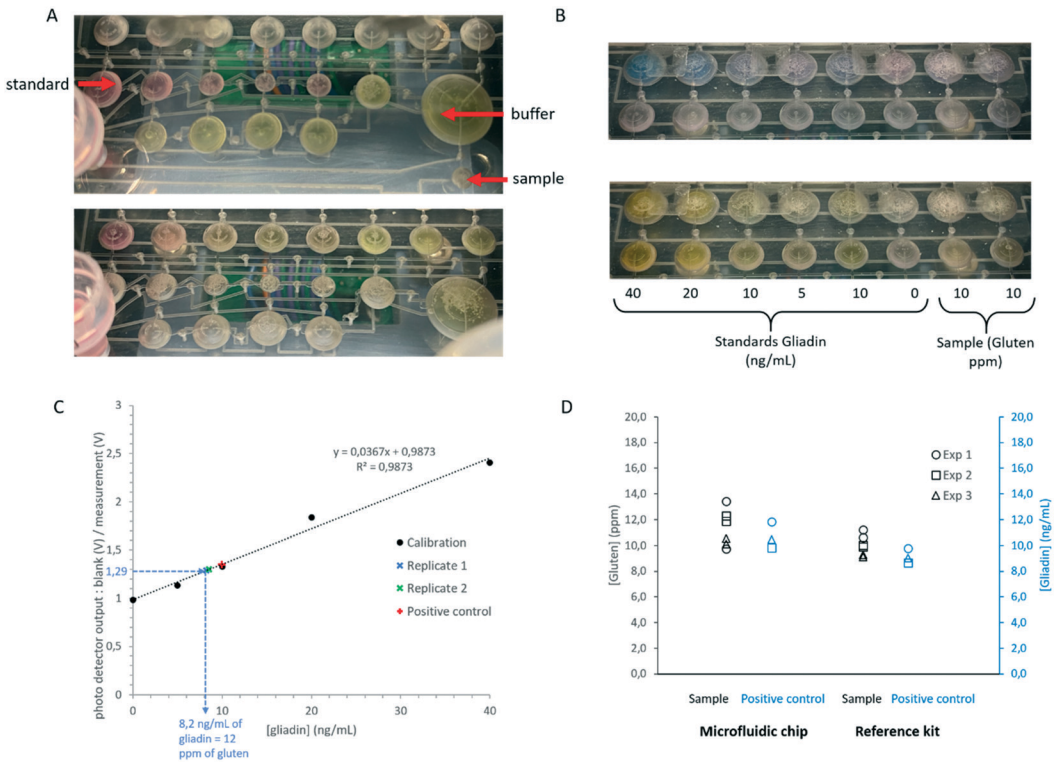

Fig. 6 Validation of an ELISA assay using the fully integrated and automated ELISA. Linear dilution was performed automatically in the chip in two steps: (A) standard, buffer and sample injection (top) followed by mixing (bottom). (B) Images of the reaction chambers after mixing with TMB (top) followed by 10 min of incubation and after mixing with the stop reagent (bottom). (C) Example of a calibration curve obtained with the microfluidic system. One sample in duplicate and a positive control are measured. (D) Results of the three experiments: sample and positive control gluten and gliadin concentration determination using the microfluidic chip and the reference kit.

ppm gluten was quantified. Standards at 40, 20, 10, 5, and 0 ng mL^{-1} gliadin were prepared in the chip by using a linear dilution architecture explained in Fig. 2 and the buffer and the 40 ng mL^{-1} gliadin solution provided in the commercial kit were mixed (Fig. 6A). After that, the protocol follows the same steps as that for the versatile architecture until the detection step (Fig. 6B). In this architecture, optical wells has been added for on chip optical detection. The solution transfer into the optical wells is crucial to avoid air bubble trapping. To limit that problem, the solutions are transferred to the optical wells at a low flow rate. To do so, we control the time evolution of the pressure applied on the membrane. This is done in a similar way to the supernatant removal protocol described previously (*i.e.* pressure steps of 2 to 10 mbar in few seconds to few minutes).

The results are obtained immediately at the end of the experiment.

The standard 10 ng mL^{-1} has been added in duplicate to be used as a positive control which assures the test validity. By using the calibration curve, the concentration of gliadin in the positive control can be calculated (Fig. 6C). If the error between the expected value and the measurement value is less than 30%, the test is assumed to be valid. The experiment has been performed three times. Errors between 2 and 18% have been found for the positive control (Fig. 6D) and the samples have been quantified with an error in the range of 15–30%. These results fulfill the criteria of acceptance given in the regulation. In addition, preliminary results using muesli show a limit of detection of 2 ppm. We also addressed the specificity and we observed no cross reactivity for gluten detection in the presence of soya in millet flour.

To be usable on field, another interest is that the entire ELISA protocol is achieved under a closed and confined format. This appears to be a clear advantage to avoid any cross contamination between various samples to be analyzed, compared to the use of microplates with a pipetting robot.

Conclusions

We established a generic microfluidic platform for the integration of complex biological protocols. The developed microfluidic architectures allow the full integration of such protocols, such as immunoassays based on magnetic bead manipulation with *ex tempo* calibration and automation. At this stage, we can consider that we have validated most of the ASSURED criteria stipulated by the WHO with the development of a sensitive, specific, user friendly, rapid and robust platform. Since we choose to integrate a complete ELISA protocol with calibration and washing steps, this makes it difficult to reach an affordable and equipment free test. Nevertheless, our compact and transportable platform is made of general use products. The last criteria (deliverable) could be validated by integrating the reagents directly in the chip, and this will be addressed in further studies.

This study demonstrated the feasibility of capture and wash steps inside a microfluidic chip, by handling magnetic beads grafted with capture molecules. Two microfluidic chip architectures have been developed and characterized. Based on the obtained results, we successfully achieved the set-up of a complete ELISA protocol with integrated optical detection. Quantitative results can be provided in less than one hour.

We successfully validated our system on a food safety application, *i.e.* gluten quantification in the dynamic range of 10 to 30 ppm with a sensitivity of 2 ppm. All the results are in agreement with the reference commercial kit and the compliance criteria required by the regulation. Other allergens of interest could be quantified using the same microfluidic platform. In addition, the use of this generic system can be easily extended to other important molecules, such as relevant biomarkers (*i.e.* troponin in cardiology) in clinics or toxins in mobile laboratories.

Conflicts of interest

"There are no conflicts to declare".

Acknowledgements

This work was supported by the Groupe Dusaussoy, the " région Hauts-de-France" and Bpifrance. The authors also acknowledge CEA for internal funding.

Notes and references

1 X. Weng and S. Neethirajan, *Trends Food Sci. Technol.*, 2017, **65**, 10–22.
2 M. Savonnet, T. Rolland, M. Cubizolles, Y. Roupioz and A. Buhot, *J. Pharm. Biomed. Anal.*, 2021, **194**, 113777.
3 D. W. Kemper, V. Semjonow, F. de Theije, D. Keizer, L. van Lippen, J. Mair, B. Wille, M. Christ, F. Geier, P. Hausfater, D. Pariente, V. Scharnhorst, J. Curvers and J. Nieuwenhuis, *Clin. Biochem.*, 2017, **50**, 174–180.
4 J. R. Choi, K. W. Yong, J. Y. Choi and A. C. Cowie, *Sensors*, 2019, **19**, 1–31.
5 S. He, N. Joseph, S. Feng, M. Jellicoe and C. L. Raston, *Food Funct.*, 2020, **11**, 5726–5737.
6 D. Gosselin, M. N. Belgacem, B. Joyard-Pitiot, J. M. Baumlin, F. Navarro, D. Chaussy and J. Berthier, *Sens. Actuators, B*, 2017, **248**, 395–401.
7 M. J. Jebrail, M. S. Bartsch and K. D. Patel, *Lab Chip*, 2012, **12**, 2452.
8 Y. Fouillet, D. Jary, C. Chabrol, P. Claustre and C. Peponnet, *Microfluid. Nanofluid.*, 2008, **4**, 159–165.
9 Y. Zhang and N. T. Nguyen, *Lab Chip*, 2017, **17**, 994–1008.
10 D. M. Bruls, T. H. Evers, J. A. H. Kahlman, P. J. W. van Lankvelt, M. Ovsyanko, E. G. M. Pelssers, J. J. H. B. Schleipen, F. K. de Theije, C. A. Verschuren, T. van der Wijk, J. B. A. van Zon, W. U. Dittmer, A. H. J. Immink, J. H. Nieuwenhuis and M. W. J. Prins, *Lab Chip*, 2009, **9**, 3504.

11 J. Park, V. Sunkara, T. H. Kim, H. Hwang and Y. K. Cho, *Anal. Chem.*, 2012, **84**, 2133–2140.
12 K. Wang, R. Liang, H. Chen, S. Lu, S. Jia and W. Wang, *Sens. Actuators, B*, 2017, **251**, 242–249.
13 J. Kim, A. Stockton, E. C. Jensen and R. A. Mathies, *Lab Chip*, 2016, **16**, 812–819.
14 C. H. Weng, K. Y. Lien, S. Y. Yang and G. Bin Lee, *Microfluid. Nanofluid.*, 2011, **10**, 301–310.
15 E. B. Bahadır and M. K. Sezgintürk, *TrAC, Trends Anal. Chem.*, 2016, **82**, 286–306.
16 J. R. Crowther, *The ELISA guidebook*, Springer, 2009, vol. 566.
17 T. Wang, M. Zhang, D. D. Dreher and Y. Zeng, *Lab Chip*, 2013, **13**, 4190.
18 M. J. Uddin, N. H. Bhuiyan and J. S. Shim, *Sci. Rep.*, 2021, **11**, 1–9.
19 B. Dai, S. Chen, W. Li, L. Zheng, X. Han, Y. Fu, J. Wu, F. Lin, D. Zhang and S. Zhuang, *Sens. Actuators, B*, 2019, **300**, 127017.
20 X. Chen, Y. Ning, S. Pan, B. Liu, Y. Chang, W. Pang and X. Duan, *ACS Sens.*, 2021, **6**, 2386–2394.
21 I. F. Pinto, R. R. G. Soares, M. E. L. Mäkinen, V. Chotteau and A. Russom, *ACS Sens.*, 2021, **6**, 842–851.
22 M. F. Abate, M. G. Ahmed, X. Li, C. Yang and Z. Zhu, *Lab Chip*, 2020, **20**, 3625–3632.
23 D. Liu, Y. Zhang, M. Zhu, Z. Yu, X. Ma, Y. Song, S. Zhou and C. Yang, *Anal. Chem.*, 2020, **92**(17), 11826–11833.
24 X. Weng, G. Gaur and S. Neethirajan, *Biosensors*, 2016, **6**, 1–10.
25 M. Zhao, X. Li, Y. Zhang, Y. Wang, B. Wang, L. Zheng, D. Zhang and S. Zhuang, *Food Chem.*, 2021, **339**, 127857.
26 M. Herrmann, E. Roy, T. Veres and M. Tabrizian, *Lab Chip*, 2007, **7**, 1546–1552.
27 S. Reza Mahmoodi, P. Xie, D. P. Zachs, E. J. Peterson, R. S. Graham, C. R. W. Kaiser, H. H. Lim, M. G. Allen and M. Javanmard, *Sci. Adv.*, 2021, **7**, 1–9.
28 J. R. Choi, J. H. Lee, A. Xu, K. Matthews, S. Xie, S. P. Duffy and H. Ma, *Lab Chip*, 2020, **20**, 4539–4551.
29 M. Ben Ismail, E. de la Serna, G. Ruiz-Vega, T. García-Berrocoso, J. Montaner, M. Zourob, A. Othmane and E. Baldrich, *Anal. Chim. Acta*, 2018, **999**, 144–154.
30 D. Tang, Y. Cui and G. Chen, *Analyst*, 2013, **138**, 981–990.
31 J. Yang, X. Xiao, L. Xia, G. Li and L. Shui, *Anal. Chem.*, 2021, **93**, 8273–8280.
32 Y. Fouillet, C. Parent, G. Gropplero, L. Davoust, J. L. Achard, F. Revol-Cavalier and N. Verplanck, *Proceedings*, 2017, **1**, 501.
33 F. Pineda, F. Bottausci, L. Malaquin and Y. Fouillet, in *MicroTAS 2015 - 19th International Conference on Miniaturized Systems for Chemistry and Life Sciences*, 2015.
34 M. Wehner, R. L. Truby, D. J. Fitzgerald, B. Mosadegh, G. M. Whitesides, J. A. Lewis and R. J. Wood, *Nature*, 2016, **536**, 451–455.
35 C. Parent, F. Boizot, M. Cubizolles, N. Verplanck, J. L. Achard and Y. Fouillet, *Sens. Actuators, B*, 2018, **261**, 106–114.
36 E. Pariset, C. Parent, Y. Fouillet, B. François, N. Verplanck, F. Revol-Cavalier, A. Thuaire and V. Agache, *Sci. Rep.*, 2018, **8**, 17762.
37 B. Shahbazkhani, M. M. Fanaeian, M. J. Farahvash, N. Aletaha, F. Alborzi, L. Elli, A. Shahbazkhani, J. Zebardast and M. Rostami-Nejad, *Sci. Rep.*, 2020, **10**, 1–8.
38 Codex Alimentarius International Food Standard, *Standard for Foods for Special Dietary Use for Persons Intolerant To Gluten Cxs 118-1979*, 2015, vol. 1.
39 B. Cortese, M. C. Mowlem and H. Morgan, *Sens. Actuators, B*, 2011, **160**, 1473–1480.
40 C. Quintard, E. Tubbs, J. L. Achard, F. Navarro, X. Gidrol and Y. Fouillet, *Biosens. Bioelectron.*, 2022, **202**, 113967.
41 I. Valdés, E. García, M. Llorente and E. Méndez, *Eur. J. Gastroenterol. Hepatol.*, 2003, **15**, 465–474.